Sulfate radical anion-based degradation of metazachlor herbicide in the water and gas: A theoretical study

Dinh Hieu Truong[a,b], Nguyen Thi Ai Nhung[c], Sonia Taamalli,[d] Abderrahman El Bakali,[d] Florent Louis,[d] Duy Quang Dao[a,b,*]

[a]*Institute of Research and Development, Duy Tan University, Da Nang 550000, Viet Nam*

[b]*Faculty of Natural Science, Duy Tan University, Da Nang 550000, Viet Nam*

[c]*Department of Chemistry, University of Sciences, Hue University, Hue City 530000, Viet Nam*

[d]*Univ. Lille, CNRS, UMR 8522, Physico-Chimie des Processus de Combustion et de l'Atmosphère, 590000 Lille, France.*

Abstract

Metazachlor (MTZ) herbicide oxidation initiated by sulfate radical anion ($SO_4^{\bullet-}$) in water and gas was investigated using the density functional theory (DFT) at the M06-2X/6-311++G(3df,3pd)//M06-2X/6-31+G(d,p) level of theory. Mechanisms and kinetics of MTZ oxidation *via* three oxidation mechanisms were investigated, including abstraction (Abs), addition (Add), and single electron transfer (SET). Results show that most oxidation reactions are favorable and spontaneous in both phases. The overall rate constants at 298.15K in water is 5.06×10^{10} M^{-1} s^{-1} whereas the one in gas is many times higher, 1.51×10^{13} M^{-1} s^{-1}. Notably, the degradation in water is non-selected with the fastest reaction being SET with 5.76×10^{9} M^{-1} s^{-1} and 11.39% of the k_{app} and Γ, respectively. On the contrary, the one in gas almost occurs *via* Abs reaction with the fastest one being Abs-H24 with k_{app} and Γ values being 1.08×10^{13} M^{-1} s^{-1} and 71.76%. In addition, the influence of temperature on the degradation kinetics is evaluated. Results show that the degradation in water increases as a function of temperature (283 to 323 K), while the drawback trend is found in the gas phase from 253 to 323 K. Diving into the chemical nature of the hydrogen abstraction processes, it is noteworthy that the most predominant Abs reactions at the methyl and methylene groups occur *via* the proton-coupled electron transfer (PCET) mechanism. Overall, the $SO_4^{\bullet-}$-based degradation is an effective and potential method for removing MTZ herbicide.

Keywords: metazachlor, sulfate radical anion, degradation, pesticides, kinetics,

**Corresponding author:* daoduyquang@duytan.edu.vn

Introduction

In recent years, due to the remarkable increase in the use of pesticides causing environmental pollution, advanced oxidation processes (AOPs)[1–5], especially sulfate radical anion-based AOPs (SR-AOPs), and hydroxyl radical-based AOPs (HO-AOPs) have been applied for pesticide degradation and mineralization. HO-AOPs are among the most popular techniques because they oxidize pesticides to organic or inorganic compounds with low- or non-toxic properties.[6,7] However, this process is only effective in an acidic environment and is not often selective with multistep reaction pathways.[8] In addition, the effectiveness of HO-AOPs is remarkably reduced due to the presence of $HO^{\bullet}$ radical scavengers, including dissolved organic materials and carbonate/bicarbonate anions.[4,9]

SR-AOPs possessing a high degradation ability are expected to have more potential than HO-AOPs. When determining the electronic potential in a Normal Hydrogen Electrode (NHE) at circum-neutral pH, the redox potential of $SO_4^{\bullet-}$ is 2.5–3.1 V compared to 1.8–2.7 V for $HO^{\bullet}$.[5,10] Besides, the half-life and the broader pH range of $SO_4^{\bullet-}$ (30–40 µs and pH = 2–8) are also higher than those of $HO^{\bullet}$ (20 ns and pH = 2–4).[11–14] Therefore, SR-AOPs may be applied to include neutral or even basic conditions. Besides, the employed oxidants in SR-AOPs, including peroxymonosulfate (PMS) and persulfate (PS), are in the solid phase, leading to being easily transported, compared to the liquid phase of H_2O_2 in HO-AOPs.[1,4] As a result, SR-AOPs are a potential alternative to HO-AOPs and thus tend to have a broader application in environmental remediation.

In SR-AOPs, the common oxidizing agents are PMS (HSO_5^-) or PS ($S_2O_8^{2-}$), which are activated to produce sulfate radical anion $SO_4^{\bullet-}$.[1,4,5] PMS agents, commonly known as Oxone – $2KHSO_5{\cdot}KHSO_4{\cdot}K_2SO_4$, are non-toxic, readily dissolved in water, and stable over a broad pH range.[4] Outstandingly, $HO^{\bullet}$ and sulfur pentoxide radicals ($SO_5^{\bullet-}$) are also formed, as well as $SO_4^{\bullet-}$, in activating PMS.[3] Meanwhile, the structure of PS agents, such as $Na_2S_2O_8$ or $K_2S_2O_8$, is symmetric, leading to increased stability and activation energy.[15] As a result, PS has a more vital oxidizing ability than PMS. In SR-AOPs, the PS/PMS needs to be activated to degrade pesticides. Popular activation techniques include catalyst-free activations (*i.e.*, UV [16], ultrasonic [17], microwave [18], heat [19], and visible light [20]) and metal-based catalyst activations (*i.e.*, transition metals[21], homogeneous[22], heterogeneous [23], photo-electrons[24], electrochemical[25], alkali[26], carbon-based materials[27], and hybrid[28]). However, each method has its advantages and disadvantages. For example, transition metal activation has low energy and high reactivity for degradation and a low cost (only 0.517$ /m^3 for Fe^{2+}), but it causes a risk of metal ion leaching.[29] In addition, many factors, such as the nature and concentration of organic matter or inorganic salts and the environmental pH, often significantly influence SR-AOP processes. As a result, activation methods should be carefully considered to choose the suitable one for each industrial wastewater based on the reality of the situation.

Besides the application of pesticide degradation in water, SR-AOPs are also one of the most popular techniques for gaseous pollutant removal due to the strong oxidation ability of $SO_4^{\bullet-}$ and the environmental friendliness of oxidation products.[30,31] Like the SR-AOPs in the water, the gaseous phase processes also use the PS or PMS as oxidizing agents, which must be activated. Generally, SR-AOPs treat various emission sources, including flue gas, biogas, nature gas, coke oven gas, coalbed methane, waste incineration tail gas, and chemical process exhaust.[30] The SR-AOPs have proven highly effective for volatile organic compounds in gaseous pollutants. In initial studies, the removal

efficiencies of SR-AOPs for gaseous pollutants removal of toluene, ethyl acetate, and chlorobenzene were determined as nearly 90%[32], 98.3%[33], and 90-97%[34], respectively.

The mechanism and kinetics of pesticide degradation by sulfate radical anions have recently been an attractive topic and have been investigated in the literature using experimental and computational approaches.[5,10,35–42] He *et al.*[35] experimentally and theoretically studied the degradation of lindane using $SO_4^{\bullet-}$ in water. Experimentally, compared with *p*–cyanobenzoic acid as a reference compound, the second order rate constant (*k*) was $(8.95 \pm 0.29) \times 10^6$ M^{-1} s^{-1}. Meanwhile, the experimental results showed that H-abstraction reactions of cyclohexane were the main ones with the highest rates. Moreover, the *k* value was 4.41×10^7 M^{-1} s^{-1}, close to the experiment. Lutze *et al*. degraded atrazine, propazine, and terbuthylazine by sulfate radical anions in reaction solutions adjusted to pH 7 with sodium hydroxide in water.[37] Results showed that the rate constants of these processes were determined as $4.5 \pm 0.30 \times 10^9$, $2.2 \pm 0.05 \times 10^9$, and $3.0 \pm 0.05 \times 10^9$ M^{-1} s^{-1}, respectively. For the atrazine oxidation by $SO_4^{\bullet-}$, de-alkylations play a crucial role with 63%, in which de-ethylation is about ten times more dominant than de-isopropylation. Besides, Luo *et al*. theoretically investigated the removal of 76 aromatic contaminants (ACs).[40] The results showed that the higher the electron-donating character of ACs is, the lower the Gibbs free energy of the single electron transfer (SET) reaction is. Furthermore, the calculated second-order rate constants for the ACs *via* the SET pathway were compared with their experimental *k* values, and two fundamental SET reaction mechanisms were proposed based on the identified intermediates. As a result, the SET pathway played the main role in the degradation of these ACs with values around 10^9 M^{-1} s^{-1}. Specifically, decarboxylation of the carboxylate group of benzoate compounds was the second favorable reaction following the SET one.

Metazachlor (MTZ) commondly named as 2-chloro-N-(2,6-dimethylphenyl)-N-((1H-Pyrazol-1-yl)methyl) acetamide is an organochlorine compound. In agriculture, MTZ acts as a herbicide to protect oil seed crops by controlling annual grass and broad-leaved weeds. Generally, it is sprayed on the soil as a pre-emergence herbicide[43,44], contaminating the aquatic environment, including surface water and groundwater. Indeed, the concentration of MTZ in both tributaries in the Navesti River in Estonia was about 0.6 ng L^{-1}.[45] The MTZ has also been found in other areas in Europe, such as Germany[46], the Czech Republic[47], and Belgium[48], with an overall concentration in water varied in the range of 0.1 µg/l – 100 µg/l. In natural water, MTZ is often detected with its oxidation products. Ulrich *et al*. showed that the MTZ, MTZ-oxalamic acid (MTZ OA), and MTZ – ethane sulfonic acid (MTZ ESA) were found in surface water in a river in the North of Germany, with the concentrations being 0.62, 1.8, and 4.8 µg L^{-1}, respectively.[49] In addition, MTZ is also measured in the air environment. Recently, Mayer *et al*. measured pesticide distribution in the European atmosphere and demonstrated that MTZ was mainly found at the coastal, nonfree tropospheric mountain, and rural sites, with the highest concentration being 2.59 ng m^{-3}.[50] As a consequence, the accumulation of MTZ in the aquatic environments leads to harmful effects on the biosystems and biodiversity. MTZ is known as moderately toxic to many types of marine species[43,51–53]. For example, the LC_{50} of MTZ for the Zebrafish (Danio rerio)[51] is determined as 5.0 mg/l, whereas its EC_{50} is 1.63 mg/l for green alga *Chlorella spp*. in 96h[52]. In addition, for mammalian, including rats, mice, and dogs, MTZ's acute

toxicity is low *via* oral, dermal, and inhalation routes with median lethal dose – LD_{50} > 2000 mg/kg and median lethal concentration – LC_{50} > 34.5 mg/L.[48]

Because of its accumulation and possible toxicity properties, the degradation of MTZ in environmental conditions has been a targeted project using experimental and theoretical approaches. Kask *et al*. have studied the sonolytic degradation of MTZ. As a result, the pseudo-first-order rate constants of MTZ degradation initiated by conventional sonolytic and O_2-saturated and Fe_2O_3-added solutions are 1.11×10^{-2} min^{-1}, and 1.79×10^{-2} and 2.88×10^{-2} min^{-1}, respectively.[45] Moreover, two degradation pathways were performed, including cleavage of the aliphatic sites and reactions of the pyrazole ring (*i.e.,* the initial hydroxylation and oxidation). Dao *et al*.[7] also investigated the MTZ oxidation by hydroxyl radicals in the gas and aqueous phases using density functional theory (DFT). Results show that the oxidation rate constants decreased from 8.40×10^{10} to 8.31×10^{9} M^{-1} s^{-1} and from 1.31×10^{9} to 1.27×10^{9} $M^{-1}s^{-1}$, respectively, with the rise of temperature from 250 to 400K. Furthermore, the authors reported that the main products resulting from the oxidation are recognized as developmental toxicants with no mutagenic toxicity using the ECOSAR approach.

Although several studies have investigated the sulfate radical anion-based oxidation of pesticides, many details of these processes are still unclear and remain enigmatic. Indeed, the mechanism, kinetics, and influencing parameters of pesticide degradation using $SO_4^{\bullet-}$ in different environments are still uncertain and need more research, especially from the computational approaches. Therefore, our primary goal in this study is to evaluate metazachlor (MTZ) herbicide degradation by sulfate radical anions in different environmental media, including the gas and the aqueous phases. The degradation mechanisms were considered *via* three processes: H-abstraction (Abs), addition (Add), and single electron transfer (SET). The temperature ranges in the gas and water are 253-323 and 283-323K, respectively. After determining the mechanistic and kinetic parameters, the half-life times of MTZ in the sulfate radical anion-based AOPs were determined.

Computational methods

All geometry optimization and harmonic vibrational frequency calculations were performed both in the gas phase and water using Gaussian 16 Rev C.01 package [54] at the M06-2X/6-311++G(3df,3pd)//M06-2X/6-31+G(d,p) level of theory. The universal solvation model based on solute electron density (SMD)[55] was used to simulate the water solution.

In this work, the mechanism and kinetics of the initial oxidation of MTZ by $SO_4^{\bullet-}$ radicals are investigated *via* abstraction (Abs), addition (Add), and single electron transfer (SET) reactions. Abs reactions occurred at all hydrogen atoms (15 sites except the H29). In contrast, the Add ones were investigated at 9 C atoms, except the C6 position, belonging to phenyl and pyrrole rings and the C=O group. The kinetics of reactions were determined using the pre-reactive complexes scheme proposed by Singleton and Cvetanovicvia[56]. The two-step mechanism is presented *via* the following reactions:

$$MTZ + SO_4^{\bullet-} \rightarrow RC, \qquad k_a \qquad \text{(R1)}$$

$$RC \rightarrow MTZ + SO_4^{\bullet-}, \qquad k_b \qquad \text{(R2)}$$

$$RC \rightarrow TS, \qquad k_c \qquad \text{(R3)}$$

Where the RC and TS are pre-reactive complexes and transition states, respectively. Thermal rate constants – k_{TST} of these reactions are calculated as the (eq.1).

$$k_{TST} = \frac{k_c k_a}{k_b} = k_c K_{a,b} \quad \text{(eq.1)}$$

The reaction rate constant in water and the gas phase was calculated in a temperature range of 283–333 K and 253–333 K, respectively, using The GPOP program[57] by employing the conventional Transition State Theory (TST). The following equations can determine k_c and K_{ab} in (eq.1):

$$k_c(T) = \kappa(T) \times \frac{k_B T}{h} \times \frac{Q_{TS}(T)}{Q_{RC}(T)} \times exp\left(-\frac{E_{TS} - E_{RC}}{k_B T}\right) \quad \text{(eq.2)}$$

$$K_{a,b}(T) = \frac{Q_{RC}(T)}{Q_{SO_4^{\bullet-}}(T) Q_{MTZ}(T)} exp\left(\frac{E_{MTZ} + E_{SO_4^{\bullet-}} - E_{RC}}{k_B T}\right) \quad \text{(eq.3)}$$

For single electron transfer reactions (SET), the reaction rate constant was calculated *via* the equation (eq.4)[58,59] with the reaction barrier ($\Delta G^{\ddagger}$) calculated through Marcus theory[60–62] (eq.5):

$$k = \sigma\kappa \frac{k_B T}{h} e^{-\Delta G^{\ddagger}/RT} \quad \text{(eq.4)}$$

$$\Delta G^{\ddagger} = \frac{\lambda}{4}\left(1 + \frac{\Delta G^0_{\text{SET}}}{\lambda}\right) \quad \text{(eq.5)}$$

For the reaction in water, the diffusion influence must be considered. This effect was calculated based on the Collin–Kimball theory[63] and the steady-state rate constant (k_D) *via* Smoluchowski[64]. The k_D was calculated as (eq.6).

$$k_D = 4\pi\, R_{AB}\, D_{AB}\, N_A \quad \text{(eq.6)}$$

Where the R_{AB} is the reaction distance, D_{AB} is the mutual diffusion coefficient of the reactants A (MTZ) and B ($SO_4^{\bullet-}$), and N_A is the Avogadro number.

The diffusion-corrected apparent rate constants (k_{app}) are then determined *via* the following equation:

$$k_{app} = \frac{k_{TST} k_D}{k_{TST} + k_D} \quad \text{(eq.7)}$$

Finally, the overall rate constant of the $SO_4^{\bullet-}$-initiated oxidation of MTZ was determined as the sum of Abs, Add, and SET reaction rate constants.

$$k_{overall} = \sum k_{app\ (Abs)} + \sum k_{app\ (Add)} + k_{app\ (SET)} \quad \text{(eq.8)}$$

SEAGrid (http:www.seagrid.org)[65–68] is acknowledged for computational resources and services for the results presented in this publication.

Results and Discussion

1. Mechanism of initiative reactions

The mechanism of the sulfate radical anion-initiated oxidation of MTZ is studied *via* three radical–molecule reaction mechanisms, including H-abstraction (Abs), Addition (Add), and single electron transfer (SET).

The optimized structures of the transition states (TSs) of Abs and Add reactions between MTZ and sulfate radical anions in water and gas are shown in **Figures 2** and **3**, respectively. Meanwhile, **Figures 4** and **5** demonstrate the ZPE-corrected relative enthalpy profile at 0 K in water and gas,

respectively. Meanwhile, the structure, HOMO – LUMO orbitals, and ESP map of MTZ are shown in the **Figure S1** of the SI file. Cartesian coordinates of all the reactant complexes (RC), TS, and product complexes (PC) involved in these pathways are resumed in **Tables S1** and **S2**, respectively, of the Supporting information (SI) file. In addition, **Figures 6** and **7** present the reaction pathway diagram of all the studied processes in the water and gas phases, respectively, in resuming their standard Gibbs free energies of reaction ($\Delta_r G^0$) and Gibbs free energies of activation ($\Delta_r G^{\neq}$).

1.1. Abstraction reaction

Abstraction reaction between MTZ and $SO_4^{\bullet-}$ occurs at all hydrogen atoms, except the H29 one, because of the existence of nearby functional groups having the steric effect that prevents $SO_4^{\bullet-}$ from interacting with this atom. As can be seen in **Figures 2** and **3**, C···H distances of the TS structures vary from 1.15 to 1.29 Å in water and from 1.25 to 1.37 Å in gas, whereas H···O ones are from 1.22 to 1.63 Å in water and from 1.09 to 1.36 Å in gas. The bond angles vary from 157 to 176º and 160 to 173º in water and gas, respectively.

Regarding Abs reactions in water, all the Abs reactions in water are barrierless, especially reactions at alkyl groups (*i.e.,* methyl and methylene). Indeed, the relative enthalpies at 0K of these TSs (ΔH_{0K}) vary from -51.7 (TS-H24) to -27.1 kJ mol^{-1} (TS-H20) in water (**Figure 4**), and the Gibbs free energies of activation $\Delta G^{\ddagger}$ values at 298.15 K varying from -0.9 (Abs-H26) to 20.8 kJ mol^{-1} (Abs-H21) (**Figure 6**). As a result, these reactions are all spontaneous and exergonic, with the standard Gibbs free energies of reaction $\Delta_r G^0$ being all negative, from -142.6 (Abs-H27, Abs-H28) to -119.0 kJ mol^{-1} (Abs-H20). The most spontaneous Abs reactions are found at Abs-H26 (ΔH_{0K} of -51.0 kJ mol^{-1} and $\Delta G^{\ddagger}$ of -0.9 kJ mol^{-1}) and Abs-H24 (ΔH_{0K} of -51.7 kJ mol^{-1} and $\Delta G^{\ddagger}$ of -0.7 kJ mol^{-1}). The standard Gibbs free energy $\Delta_r G^0$ of these two Abs reactions is equal to -140.0 kJ mol^{-1}. This can be explained by the presence of hydrogen bonds formed by one hydrogen atom close to oxygen ones of the $SO_4^{\bullet-}$ in the TS structure. Indeed, the distance for the H33(MTZ)···O38($SO_4^{\bullet-}$) and H33(MTZ)···O39($SO_4^{\bullet-}$) of the TS-H24 structure are 2.31 and 2.54 Å, respectively, while the H20(MTZ)···O39($SO_4^{\bullet-}$) and H20(MTZ)···O40($SO_4^{\bullet-}$) distances of the TS-H26 are 2.55 and 2.54 Å, respectively. As a result, the TS structure of these reactions becomes more stable, leading to a decrease in their energy barriers. Their rate constants are thus expected to be very fast. On the contrary, Abs reactions at hydrogen sites belonging to benzene and pyrrole rings have significantly higher ΔH_{0K} and $\Delta G^{\ddagger}$ at 298.15 K. ΔH_{0K} values of the TSs vary from -22.4 (TS-H22) to 6.9 kJ mol^{-1} (TS-H31) (**Figure 4**). Consequently, these Abs reactions may be slower than ones at methyl and methylene sites.

Regarding the degradation in the gas phase, Abs reactions at alkyl groups of MTZ are also the most spontaneous and exergonic reactions. ΔH_{0K} values for the TSs vary from -39.4 (TS-H24) to -13.1 kJ mol^{-1} (TS-H28) (**Figure 5**), while $\Delta G^{\ddagger}$ ones at 298.15 K are from 11.4 (Abs-H24) to 37.2 (Abs-H28), and $\Delta_r G^0$ ones vary from -77.6 (Abs-H24) to 51.7 kJ mol^{-1} (Abs-H31) (**Figure 6**). Among them, the Abs reaction at H24 has the lowest ΔH_{0K} of the TS as well as $\Delta G^{\ddagger}$ at 298.15 K, due to the formation of the hydrogen bond H32(MTZ)···O38($SO_4^{\bullet-}$), with the distance being 2.13 Å. This reaction may play the most crucial role in the degradation of MTZ in the gas phase. Meanwhile, the

Abs reactions at benzene and pyrrole rings have higher ΔH_{0K} of the TS and $\Delta G^{\ddagger}$ at 298 K and may have significantly slow rates compared to those at alkyl groups.

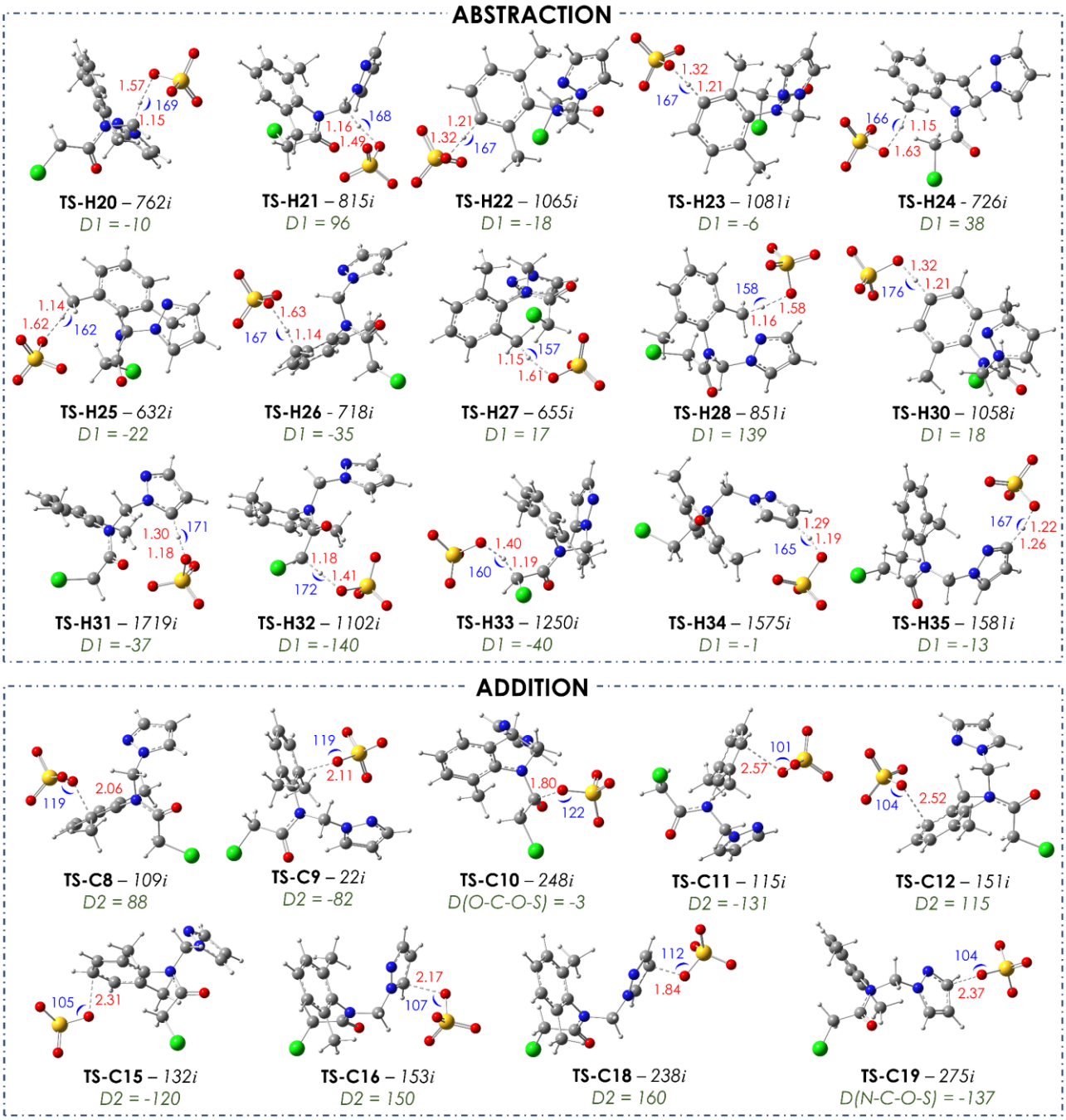

Figure 2: Optimized structure of the transition states (TSs) for the hydrogen abstraction (Abs) and addition (Add) reactions between metazachlor (MTZ) and sulfate radical anion ($SO_4^{\bullet-}$) in water. Numbers in red, blue, and green colors are interactive distances (Å), interactive angles (º), and interactive dihedral angles (º), respectively. D1 and D2 are C-H-O-S and C-C-O-S dihedral angles, respectively. The imaginary frequencies are also indicated.

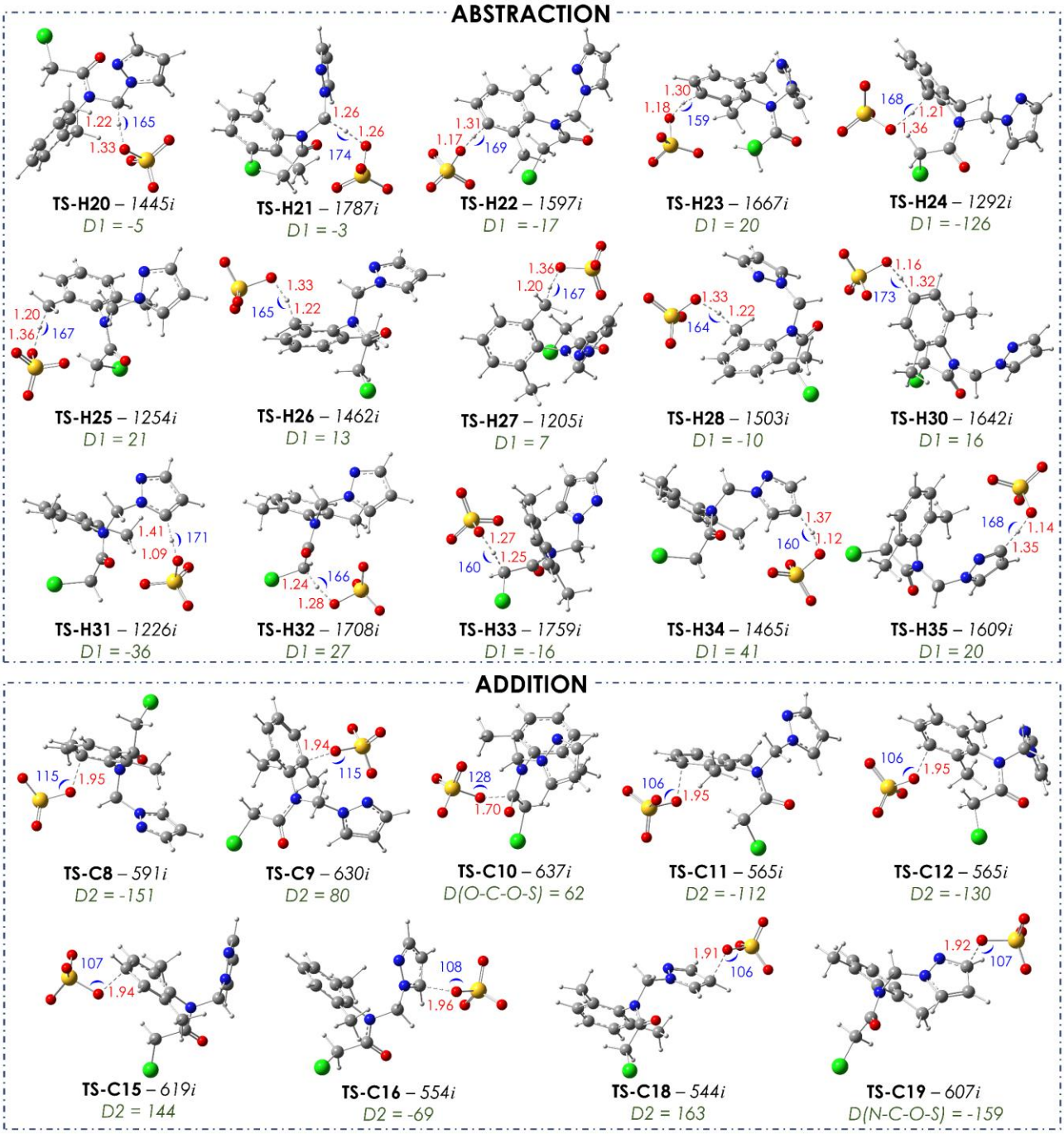

Figure 3: Optimized structure of the transition states (TSs) for the hydrogen abstraction (Abs) and addition (Add) reactions between metazachlor (MTZ) and sulfate radical anion ($SO_4^{\bullet-}$) in the gas phase. Numbers in red, blue, and green colors are interactive distances (Å), interactive angles (º), and interactive dihedral angles (º), respectively. D1 and D2 are C-H-O-S and C-C-O-S dihedral angles, respectively. The imaginary frequencies are also indicated.

Thus, the Abs reactions at the H24 and H26 positions with low energy barriers are expected to be spontaneous and favorable, having high-rate constants, and may play an essential role in the degradation of MTZ by $SO_4^{\bullet-}$.

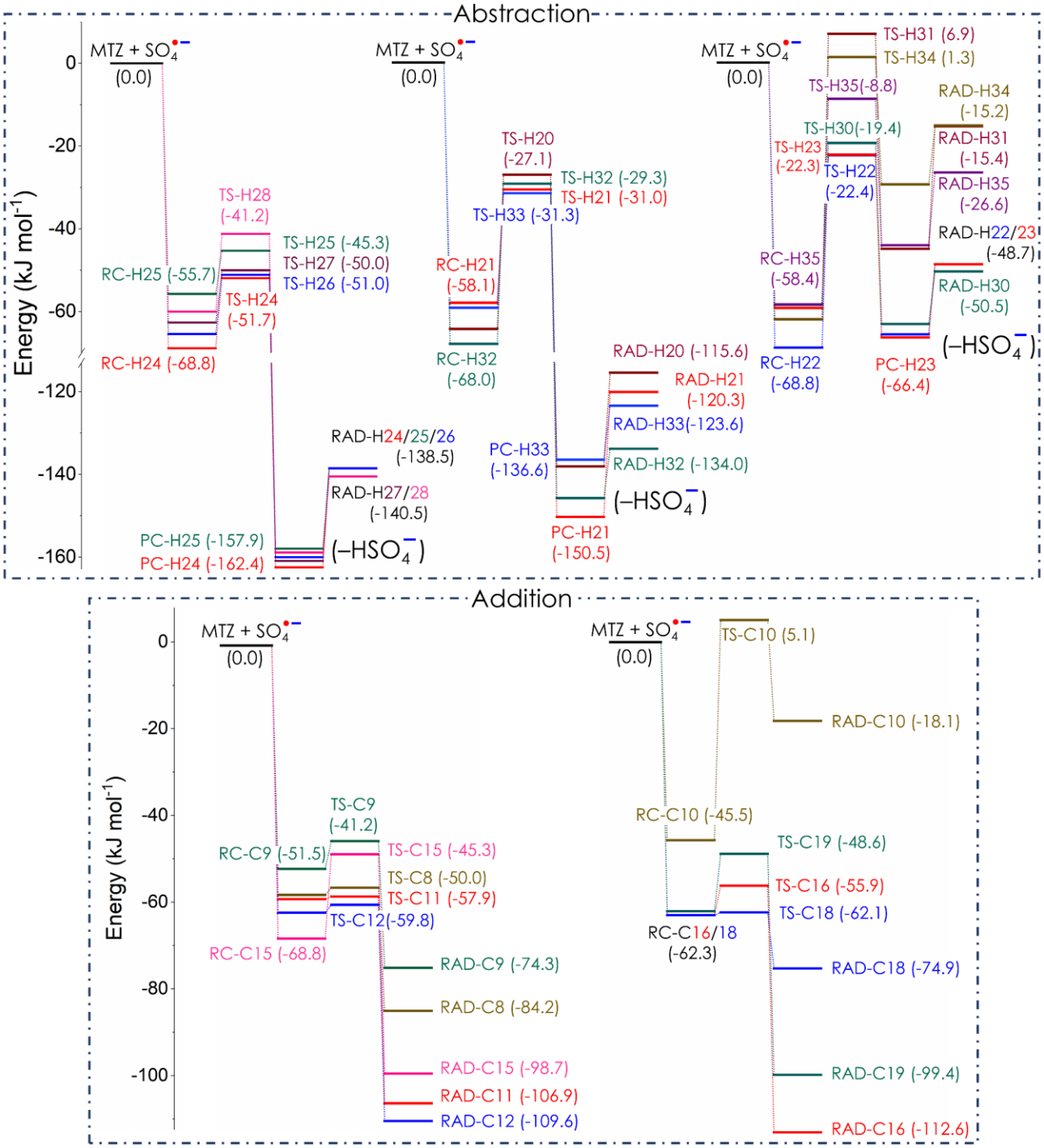

Figure 4: ZPE-corrected relative enthalpy profile at 0 K (ΔH_{0K}) for abstraction (Abs) and addition (Add) reactions initiated by $SO_4^{\bullet-}$ radical anion in water.

1.2. Addition reaction

The $SO_4^{\bullet-}$ radical may also react with MTZ *via* addition reactions (Add) at double bonds of the benzene and pyrazole rings. Regarding their TS structures in **Figures 2** and **3**, the $O(SO_4^{\bullet-})\cdots C(MTZ)$ distances vary from 1.80 to 2.57 Å in water and from 1.70 to 1.96 Å in gas.

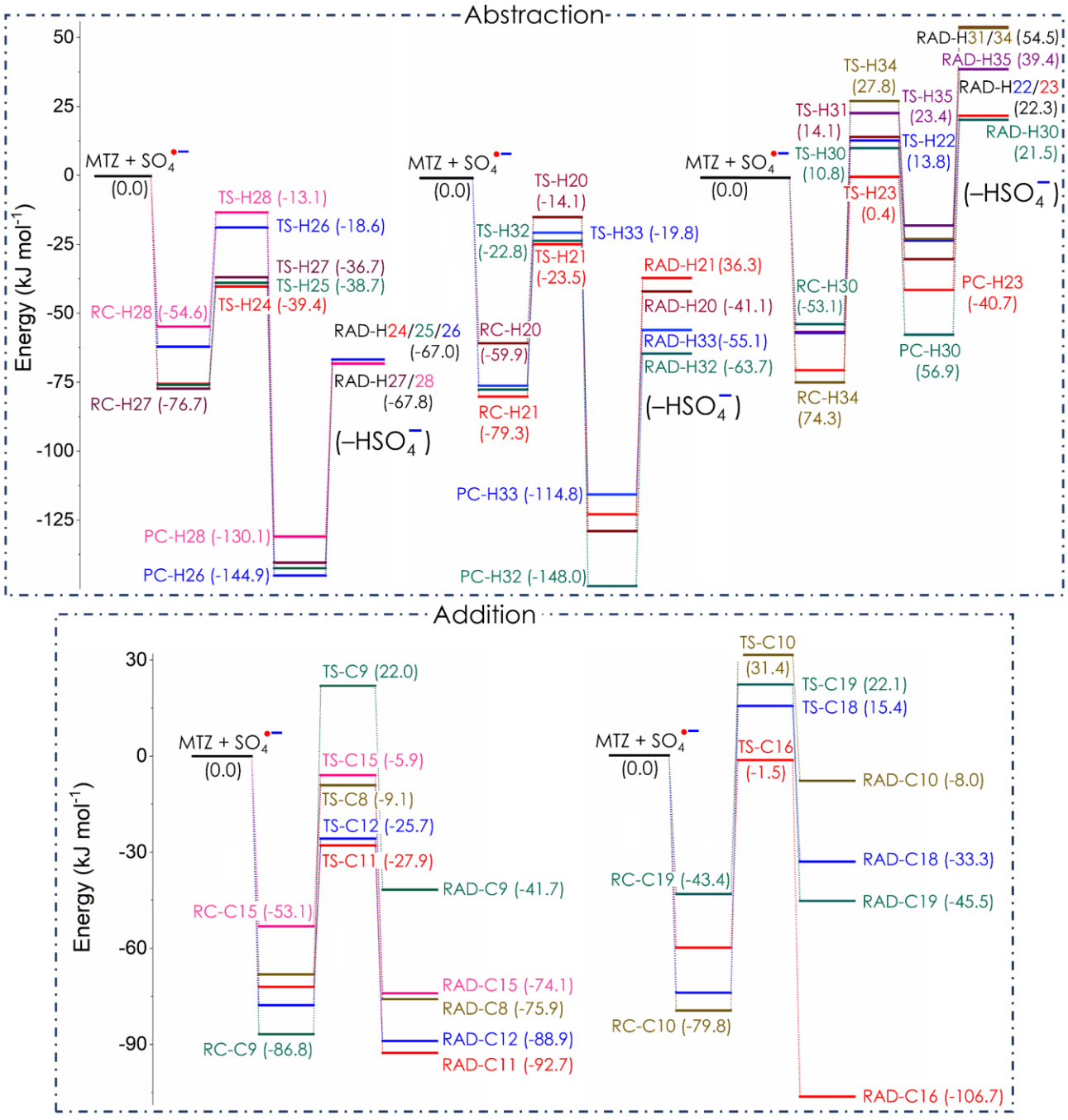

Figure 5: ZPE-corrected relative enthalpy profile at 0 K (ΔH_{0K}) for addition and abstraction reactions initiated by $SO_4^{\bullet-}$ radical in the gas

For the Add reaction in water, the reactions at benzene and pyrazole rings are represented by negative $\Delta H_{0K(TS)}$ values varying from -59.8 (TS-C12) to -41.2 kJ mol^{-1} (TS-C9), and from -62.1 (TS-C18) to -48.6 (TS-C19), respectively (**Figure 4**). As a result, the thermodynamic parameters of these reactions at 298.15 K and 1 atm condition are also relatively low. The $\Delta G^{‡}$ at 298.15 K values are from -10.9 (Add-C18) to 10.4 kJ mol^{-1} (Add-C9), whereas the $\Delta_r G^0$ ones vary from -60.4 (C16) to -14.7 kJ mol^{-1} (Add-C9), which indicates the spontaneous and exergonic properties (**Figure 7**). On the contrary, despite having the negative $\Delta_r G^0$ (-39.9 kJ mol^{-1}), the Add-reaction at C10 of the C=O group (Add-C10) is expected to be negligible because of having very high barrier energy. Indeed, its ΔH_{0K} of the TS and $\Delta G^{‡}$ at 298.15K values are 31.4 and 57.5 kJ mol^{-1}, respectively. Thus, its role in the degradation may be limited.

Regarding the Add reactions in the gas phase, the energy barriers of the Add reactions in the gas phase are higher than those in water. Indeed, the ΔH_{0K} values of the TS for the reactions at benzene and pyrazole rings are from -27.9 (TS-C11) to 22.0 kJ mol^{-1} (TS-C9) and -1.5 (TS-C16) to 22.1 kJ mol^{-1} (TS-19), respectively. Moreover, these reactions also have high $\Delta G^{‡}$ values at 298.15 K, being from 21.8 (Add-C11) to 74.8 kJ mol^{-1} (Add-C9) and from 44.3 (Add-C16) to 69.0 kJ mol^{-1} (Add-C19), respectively. Meanwhile, the Add-C10 is also insignificant because of the high energy barrier (ΔH_{0K} of the TS being 31.4 kJ mol^{-1} and 89.0 kJ mol^{-1} of $\Delta G^{‡}$). These values are all significantly higher than the corresponding values in water as well as those of Abs reactions in gas. As a result, the contribution of Add reactions in the gas phase is expected to be trivial.

To sum up, the degradation of MTZ by $SO_4^{\bullet -}$ *via* Add reactions is spontaneous and favorable in the aqueous phase with low standard Gibbs free energies of reaction and Gibbs free energies of activation. However, because of their higher energy barrier in the gas phase compared to the ones of Abs reactions, the role of the Add reactions in this phase is expected to be minor.

Outstandingly, one can see that energy barriers in water are significantly lower than the corresponding ones in the gas phase for both Abs and Add reactions. This can be explained by the better stabilization of the TS under the influence of the water solvent. Previous studies in the literature [69–71] showed that for a TS structure with high charge separation, the polar solvents with a high dielectric constant would stabilize the TS and promote the reaction to occur more favorably. As can be seen, the TS structures have a negative charge (-1), which is separated from the MTZ molecule and the sulfate radical anion, whose complexes are stabilized by the high dielectric constant of water solution (ε=78.3553). In other words, the interaction between TSs and the water molecules tends to neutralize the charge of the TSs, making them more stable. As a result, the energies of TS and the energy barriers remarkably decrease. In contrast, the TS structures in the gas phase do not have this effect and, thus, have higher energy barriers.

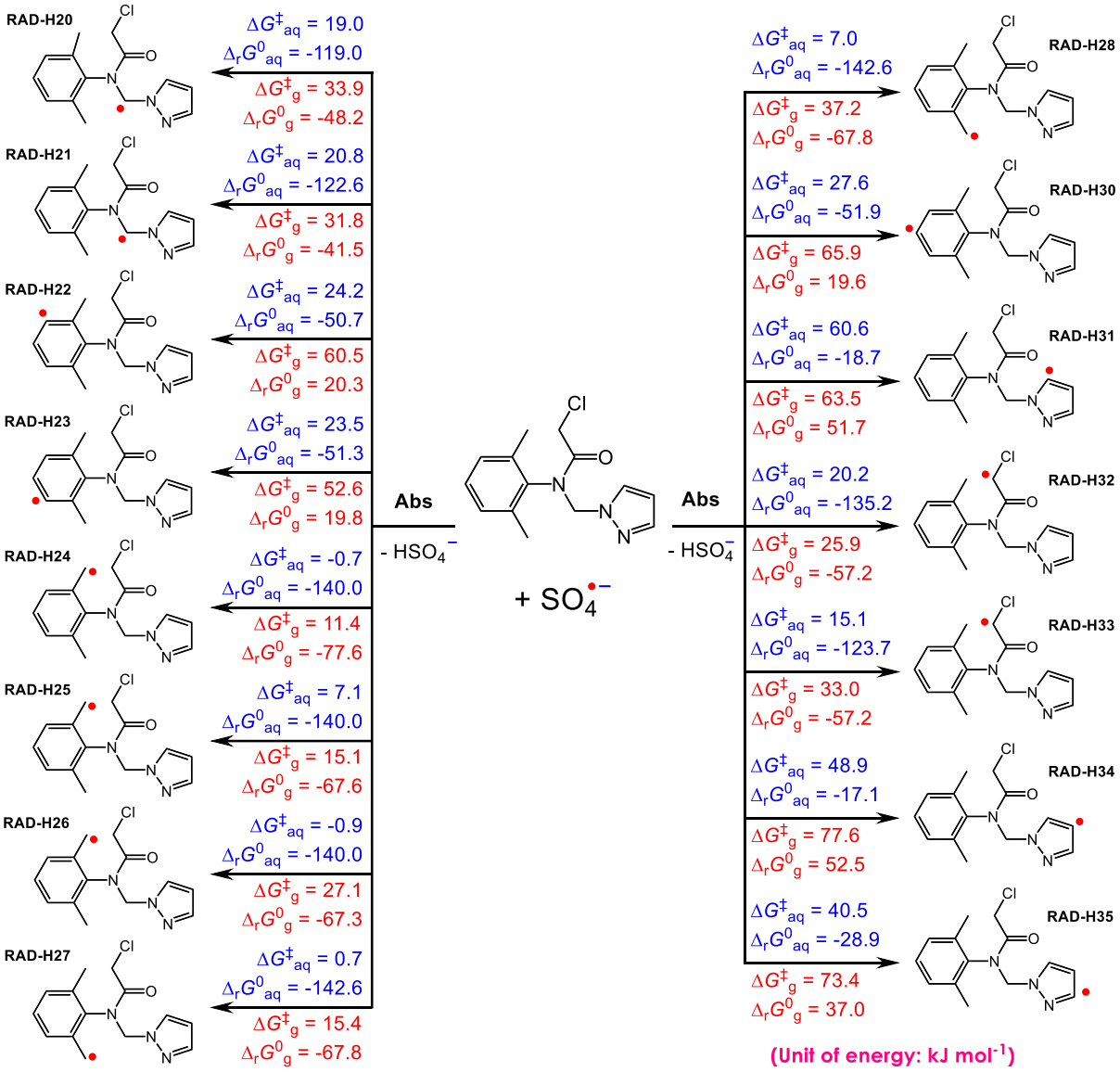

Figure 6: Schematic diagram of $SO_4^{\bullet-}$-initiated oxidation of metazachlor *via* abstraction (Abs) reactions in water (in blue) and in the gas phase (in red) at 298.15 K. Δ_rG^0 and $\Delta G^{\ddagger}$ are standard Gibbs free energies of reaction and Gibbs free energies of activation, respectively.

1.3 Single electron transfer

The single electron transfer (SET) reaction is evaluated *via* one electron donating process from MTZ to $SO_4^{\bullet-}$. As a result, in water, the SET has a relatively low energy barrier at 298.15K, with Δ_rG^0 and $\Delta G^{\ddagger}$ being 29.16 and 21.80 kJ mol^{-1}, respectively (**Figure 6**). On the contrary, the SET reaction in the gas has high values of Δ_rG^0 (226.1 kJ mol^{-1}) and $\Delta G^{\ddagger}$ (571.1 kJ mol^{-1}). Consequently, this gaseous reaction is expected to be negligible and unfavorable.

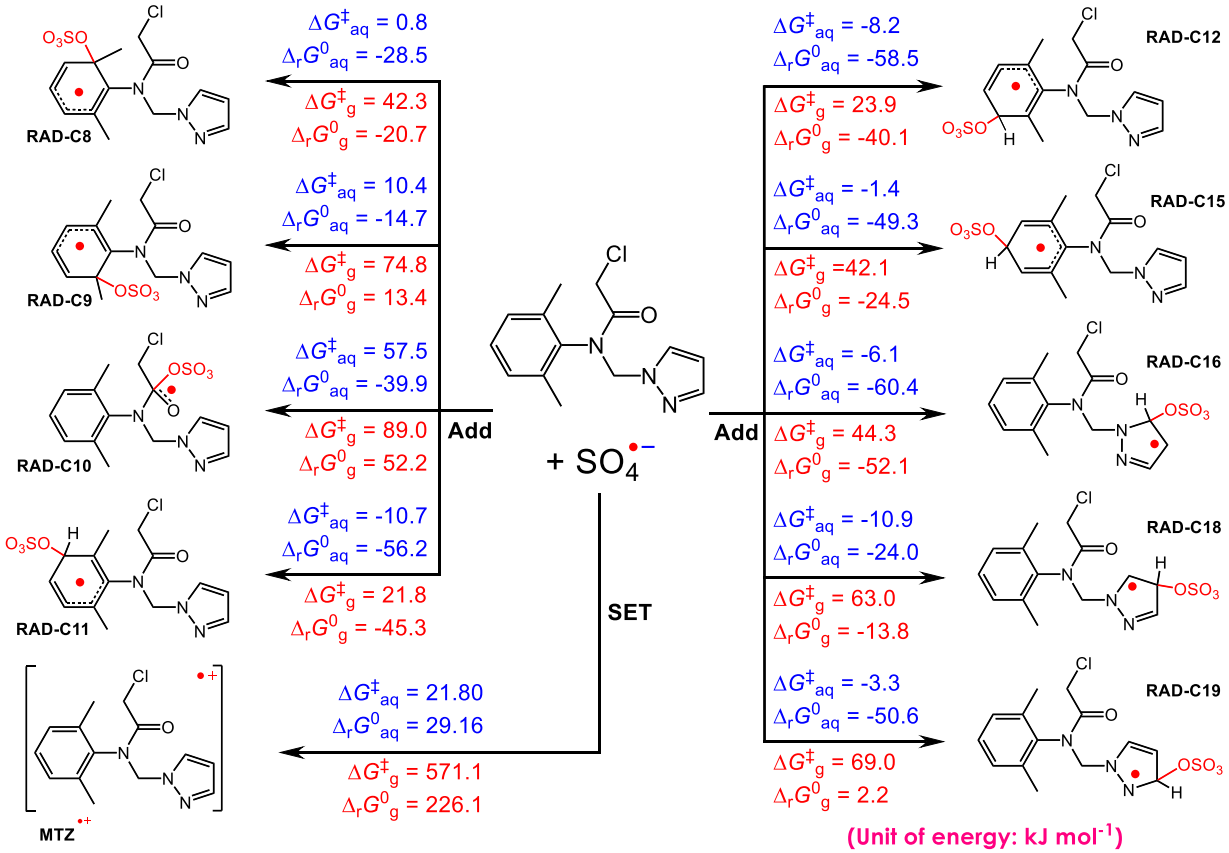

Figure 7: Schematic diagram of $SO_4^{\bullet-}$-initiated oxidation of metazachlor *via* single electron transfer (SET) and addition (Add) and reactions in water (in blue) and gas (in red) phases at 298.15 K. $\Delta_r G^0$ and $\Delta G^{\ddagger}$ are standard Gibbs free energies of reaction and Gibbs free energies of activation, respectively.

2. Kinetics of reactions

Table 1 displays the rate constants of all Add, Abs, and SET reactions between $SO_4^{\bullet-}$ radical anion and MTZ at 298.15 K in water and gas phases.

Regarding the Abs reactions in water (**Table 1**), their thermal rate constants (k_{TST}) are much larger than the corresponding diffusion rate constants (k_D) due to their low barrier energies, except the Abs ones at H31, H34, and H35. Therefore, their apparent rate constants (k_{app}) are approximately diffusion-controlled rate constants, varying from 1.80×10^9 (Abs-H30) to 2.53×10^9 M^{-1} s^{-1}(Abs-H26), with the corresponding branching ratios (Γ) being from 3.56% (Abs-H30) to 5.01% (Abs-H26), compared to the total rate constant. On the contrary, the rate constants of Abs-H31, Abs-H34, and Abs-H35 reactions are significantly lower, from 1.94×10^5 to 1.99×10^8 M^{-1} s^{-1}, with the branching ratios lower than 0.4%. In general, the Abs reactions play the most critical role, with 55.99% of the total Γ. For the reactions in the gas phase, it is noteworthy that the Abs reaction is also the most important channel. Indeed, Abs-H24, Abs-H25, and Abs-H27 are the fastest reactions in gas, with the rate constants being 1.08×10^{13}, 2.15×10^{12}, and 1.69×10^{12} M^{-1} s^{-1}, respectively. These reactions are incredibly high because the reactions in the gas phase are not influenced by the diffusion regime. Therefore, these reactions in gas are not limited by the diffusion rate like those in water. Accordingly, these reactions

possess high branching ratios, 71.76, 14.24, and 11.17%, respectively. Meanwhile, the other Abs reactions have lower rate constants varying from 6.40×10^{1} (H34) to 2.79×10^{11} M^{-1} s^{-1} (H32), and thus, their branching ratios are from 0.00% (H34) to 1.84% (H32). Overall, the total branching ratios of Abs-reaction in the gas at 298.15 K is remarkably high, with 99.69%.

Table 1. Diffusion rate constants (k_D, M^{-1} s^{-1}), thermal rate constants (k_{TST}, M^{-1} s^{-1}), apparent rate constants (k_{app}, M^{-1} s^{-1}), and branching ratio (Γ, %) of the initiative reactions between $SO_4^{\bullet-}$ radical and metazachlor in water and gas phases at 298.15 K.

	k_D	k_{TST}	k_{app}	Γ	k_{TST}	Γ
	WATER				**GAS**	
Abstraction reactions						
Abs-H20	2.48×10^{9}	6.78×10^{10}	2.40×10^{9}	4.74	2.53×10^{9}	0.02
Abs-H21	2.42×10^{9}	7.08×10^{10}	2.34×10^{9}	4.63	4.06×10^{10}	0.27
Abs-H22	2.31×10^{9}	3.23×10^{10}	2.16×10^{9}	4.27	7.81×10^{4}	0.00
Abs-H23	2.31×10^{9}	4.32×10^{10}	2.19×10^{9}	4.34	5.59×10^{6}	0.00
Abs-H24	2.53×10^{9}	3.44×10^{14}	2.53×10^{9}	5.00	1.08×10^{13}	71.76
Abs-H25	2.51×10^{9}	1.25×10^{13}	2.51×10^{9}	4.96	2.15×10^{12}	14.24
Abs-H26	2.53×10^{9}	3.73×10^{14}	2.53×10^{9}	5.01	3.89×10^{10}	0.26
Abs-H27	2.49×10^{9}	1.74×10^{14}	2.49×10^{9}	4.92	1.69×10^{12}	11.17
Abs-H28	2.47×10^{9}	1.90×10^{13}	2.47×10^{9}	4.88	7.48×10^{8}	0.00
Abs-H30	2.33×10^{9}	7.91×10^{9}	1.80×10^{9}	3.56	2.51×10^{6}	0.00
Abs-H31	2.28×10^{9}	1.94×10^{5}	1.94×10^{5}	0.00	7.03×10^{3}	0.00
Abs-H32	2.37×10^{9}	1.78×10^{11}	2.34×10^{9}	4.63	2.79×10^{11}	1.84
Abs-H33	2.35×10^{9}	1.85×10^{12}	2.34×10^{9}	4.64	2.08×10^{10}	0.14
Abs-H34	2.26×10^{9}	6.46×10^{6}	6.44×10^{6}	0.01	6.40×10^{1}	0.00
Abs-H35	2.26×10^{9}	2.18×10^{8}	1.99×10^{8}	0.39	5.12×10^{2}	0.00
Addition reaction						
Add-C8	1.89×10^{9}	1.12×10^{14}	1.89×10^{9}	3.74	8.70×10^{6}	0.00
Add-C9	1.94×10^{9}	2.35×10^{12}	1.94×10^{9}	3.84	1.79×10^{1}	0.00
Add-C10	1.65×10^{9}	1.37×10^{4}	1.37×10^{4}	0.00	5.80×10^{-2}	0.00
Add-C11	2.36×10^{9}	1.16×10^{16}	2.36×10^{9}	4.66	3.25×10^{10}	0.21
Add-C12	2.32×10^{9}	4.33×10^{15}	2.32×10^{9}	4.58	1.38×10^{10}	0.09
Add-C15	2.13×10^{9}	2.80×10^{14}	2.13×10^{9}	4.20	9.74×10^{6}	0.00
Add-C16	1.99×10^{9}	1.82×10^{15}	1.99×10^{9}	3.94	3.70×10^{6}	0.00
Add-C18	1.69×10^{9}	1.15×10^{16}	1.69×10^{9}	3.34	1.87×10^{3}	0.00
Add-C19	2.18×10^{9}	6.31×10^{14}	2.18×10^{9}	4.31	1.81×10^{2}	0.00
Single electron transfer						
SET	7.69×10^{9}	2.30×10^{10}	5.76×10^{9}	11.39	~0.00	0.00
Total						
			5.06×10^{10}	100.00	1.51×10^{13}	100.00

For the Add reactions in water, it is noteworthy that all reaction rates, except for the reaction at the C10 position of the C=O group, occur rapidly with rate constants close to the diffusion limit, from 1.69×10^9 (Add-C18) to 2.36×10^9 M^{-1} s^{-1} (Add-C11), which are corresponding to the branching ratios slightly varied from 3.34% (Add-C18) to 4.66% (Add-C11). In contrast, the k_{app} value at C10 is only 1.37×10^4 M^{-1} s^{-1} (Γ, 0.00%). The total Γ of the Add channel is equal to 32.61%. Concerning Add reactions in the gas phase, the rate constants of some Add reactions are relatively high, from 5.80×10^{-2} (Add-C10) to 3.25×10^{10} M^{-1} s^{-1} (Add-C11). However, the rate constants of the Add reactions are remarkably lower than those of Abs ones, and thus, their total branching ratio in the gas phase is only 0.30%.

Regarding the SET reaction, as mentioned above, due to the low barrier energies at 298.15 K, its thermal rate constant (k_{TST}) in water reaches 2.30×10^{10} M^{-1} s^{-1}. Moreover, because of the highest diffusion rate constants (k_D) being 7.69×10^9 M^{-1} s^{-1}, its apparent rate constant (k_{app}) is determined to be 5.76×10^9 M^{-1} s^{-1} (the corresponding branching ratio being 11.39%). As expected, the electron transfer process in the aqueous phase plays an important role in the oxidation process initiated by $SO_4^{\bullet -}$, which has usually been forgotten in several computational works in the literature, leading to a significant underestimation of the pesticides' degradation by $SO_4^{\bullet -}$ radical anion [36,41,69]. Furthermore, our observation agrees with the experimental works, which mentioned the high oxidation potential of $SO_4^{\bullet -}$ in water by quickly donating an electron to organic contaminants. [4,5,10] The SET process is predominant in the degradation of various organic compounds, notably aromatic compounds, such as phenol, aminophenol, dihydroxyl phenol[38], tyrosol[39], and anthracene[42]. In this work, this process is observed to be crucial in the degradation using $SO_4^{\bullet -}$ of the MTZ in the aqueous phase. On the contrary, the SET reaction in the gas phase is negligible because of its significantly high barrier energy, as mentioned above.

Overall, the sulfate radical anion-initiated oxidations of MTZ at 298.15 K are extremely fast in both the water and gas phases. The Abs reactions are the main channel for degradation in two phases, with the total branching ratios being 55.99 and 99.69%. In addition, it can be seen that the total rate constant in the gas (1.51×10^{13} M^{-1} s^{-1}) is about 300 times faster than that in the water (5.06×10^{10} M^{-1} s^{-1}). This can be explained by the diffusion effect of water solvent, which significantly reduces the reaction rate in water. Indeed, diffusion rate constants – k_D in water are from 1.69×10^9 to 2.23×10^9 M^{-1} s^{-1} for the Abs and Add reaction and 7.69×10^9 M^{-1} s^{-1} for the SET reaction. Hence, despite having extremely high thermal rate constants, the k_{app} values of these reactions calculated *via* (eq.7) are all lower than 2.23×10^9 M^{-1} s^{-1} for Abs and Add reactions and only 5.76×10^9 M^{-1} s^{-1} for SET reaction. For example, the Abs reactions at H24 and H26 have the k_{TST} being 3.44×10^{14} and 3.73×10^{14} M^{-1} s^{-1}, respectively, but their k_{app} values are only 2.53×10^9 M^{-1} s^{-1}. On the contrary, reactions in the gas phase are not affected by the diffusion regime of the solution, which leads to the thermal rate constants not being decreased. Among them, the rate constants of some reactions are many times higher than that in water, such as Abs-H24 ($k_{TST} = 1.08 \times 10^{13}$ M^{-1} s^{-1}) or Abs-H25 ($k_{TST} = 2.15 \times 10^{12}$ M^{-1} s^{-1}). As a result, the rate constant of a similar reaction in the gas phase is remarkably faster than that in the aqueous phase.

Finally, compared with the $SO_4^{\bullet-}$-initiated degradations in water of other compounds, the rate constant MTZ one is about 16 times higher than that of toluene (3.1×10^9 M^{-1} s^{-1})[33], 5 times than sulfamethoxazole ($12.5 \pm 1.9 \times 10^9$ M^{-1} s^{-1}) and diclofenac ($9.2 \pm 0.6 \times 10^9$ M^{-1} s^{-1})[70], and 50 times than aniline (~10^9 M^{-1} s^{-1})[71].

3. Influence of temperature on the reaction kinetics

The influences of temperature on the main reactions of the degradation in water and gas are shown in **Figures 8** and **9**, respectively. Meanwhile, all details of the rate constants and branching ratios are present in **Tables S3** to **S6** of the SI file.

Figure 8 shows the influence of temperature on the rate constant of the MTZ oxidation initiated by $SO_4^{\bullet-}$ radical anion, evaluated from 283 to 323K in water.

Regarding the degradation in water, one can see that the effect of temperature on the SET reaction is the most remarkable. Indeed, the rate constants significantly increase from 3.43×10^9 M^{-1} s^{-1} (at 283 K) to 1.14×10^{10} M^{-1} s^{-1} (at 323 K). Correspondingly, its branching ratio rises from 10.37% (283 K) to 12.96% (323 K). Similarly, almost all rate constants of Abs reactions also increase with the total rate of this channel from 1.89×10^{10} (283 K) to 5.09×10^{10} M^{-1} s^{-1} (323K) and the branching ratios varying from 57.20 to 53.63%, respectively. The k_{app} values of the most significant Abs reactions (*i.e.*, Abs-H24 and Abs-H26) increase from 1.64×10^9 and 1.65×10^9 M^{-1} s^{-1} (at 283K) to 4.49×10^9 and 4.50×10^9 M^{-1} s^{-1} (at 323 K), respectively. Similarly, all Add reactions become faster with the increase of temperature, with the total rate constant being 1.07×10^{10} and 2.93×10^{10} M^{-1} s^{-1} at 283 and 323 K, respectively. The fastest Add reaction (*i.e.,* Add-C11) occurs with the rate constant varying from 1.53×10^9 (283K) to 4.18×10^9 M^{-1} s^{-1} (323K) and the corresponding Γ being 4.63 and 4.78%, respectively. On the contrary, some reactions have drawbacks in the temperature range, including Abs-H31, Abs-H34, and Abs-H35. However, the contribution of these reactions is negligible, with the Γ from 0.00 to 0.82%.

Overall, it is noteworthy that all the reactions between MTZ and $SO_4^{\bullet-}$ in water occur with high reaction rates in the diffusion limit in the temperature range from 283 to 323 K. In addition, the k_{app} of this degradation significantly increases in this temperature range which can be explained by the increase of the diffusion rate (or the steady-state rate constant) k_D as a function of the mutual diffusion coefficient – D_{AB} (eq.6). Indeed, for the Abs and Add reactions, the k_D values at 283 K vary from 1.07×10^9 to 1.65×10^9 M^{-1} s^{-1}, whereas the ones at 323 K are from 2.93×10^9 to 4.50×10^9 M^{-1} s^{-1}. Meanwhile, the k_D values of SET reaction at 283 and 323 K are 5.00×10^9 and 1.37×10^{10} M^{-1} s^{-1}. Moreover, the k_{app} values of the main reactions in this degradation mainly depend on the k_D because their k_{TST} are many times higher than the corresponding k_D, as mentioned in the previous section. For example, the k_{TST} values of fastest reactions, *i.e.,* SET, Abs-H24, and Abs-H26 at 283 K are 1.09×10^{10}, 9.84×10^{14}, and 1.04×10^{15} M^{-1} s^{-1}, respectively, whereas ones at 323 K are 6.74×10^{10}, 7.59×10^{13}, and 3.43×10^{13} M^{-1} s^{-1}, respectively. As a result, the total rate of this degradation in water is diffusion-controlled in increasing from 3.31×10^{10} at 283 K to 8.76×10^{10} M^{-1} s^{-1} at 323 K.

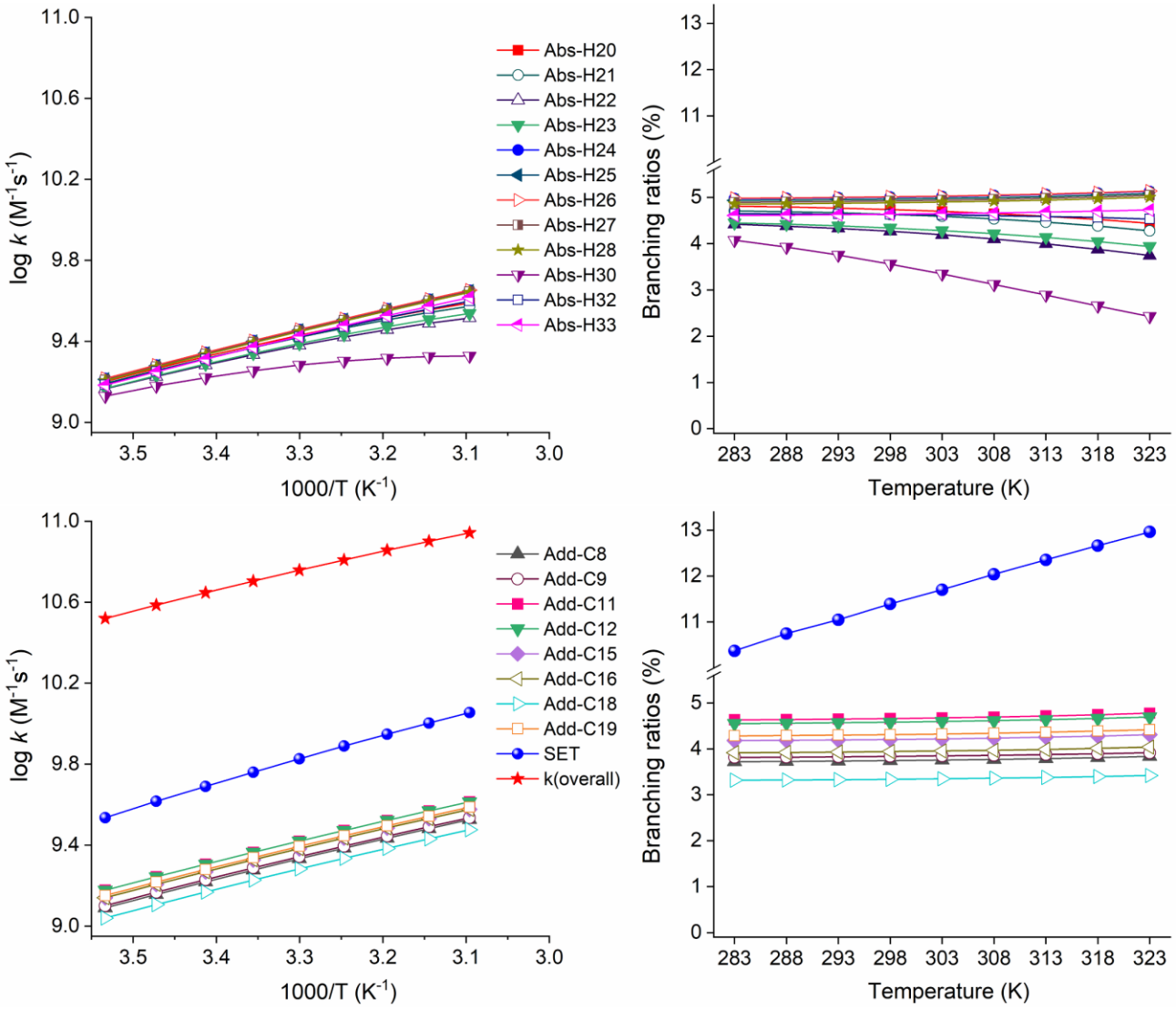

Figure 8: Influence of temperature on the rate constants described as log k (M^{-1} s^{-1}) and branching ratio Γ (%) for the most dominant abstraction (Abs), addition (Add), and SET reactions of MTZ oxidation by $SO_4^{\bullet-}$ radical in water at 283-323 K temperature range.

Regarding the degradation in the gas phase, the influence of temperature on the primary reactions of the MTZ oxidation by $SO_4^{\bullet-}$ is investigated from 253 to 323K and shown in **Figure 9**.

The rate constants of main reactions in the gas phase remarkably decrease as a function of temperature. Indeed, the rate constants of the three fastest reactions, *i.e.*, Abs-H24, Abs-H25, and Abs-H27, reduce approximately 126, 116, and 85 times, respectively. The k_{TST} values of these reactions at 253 K are 3.42×10^{14}, 6.40×10^{13}, and 4.04×10^{13} M^{-1} s^{-1}, respectively, whereas ones at 323 K are 2.71×10^{12}, 5.52×10^{11}, and 4.76×10^{11} M^{-1} s^{-1}, respectively. These reactions play the most crucial role in the degradation in the studied temperature range. Their corresponding branching ratios at 253 K are 74.53, 13.94, and 8.79%, respectively, whereas the ones at 323 K are 70.07, 14.24, and 12.30%,

respectively. Overall, a sharp decrease in all reaction rate constants is recognized in the temperature range from 253 to 323K. This observation can be explained as the equilibrium constants of these reactions, featuring the ability to convert the reactants to pre-reactive complexes (RC), decrease more rapidly than the ones of thermal rate constants when the temperature rises from 253 to 323K. For example, the equilibrium constant ($K_{A,B}$) of the Abs-H24 reaction, which accounts for more than 70% of the branching ratio, decreases about 1300 times (from 7.35×10^{-13} to 5.64×10^{-16}, respectively). In contrast, its thermal rate constant (k_c) only increases about 10 times (from 4.66×10^{26} to 4.81×10^{27} M^{-1} s^{-1}, respectively). Consequently, the k_{app} of this reaction calculated as the product of these two values reduces about 126 times, from 3.42×10^{14} (253 K) to 2.71×10^{12} M^{-1} s^{-1} (323 K). As a similar trend, other main reactions drop significantly, from 12 to 186 times.

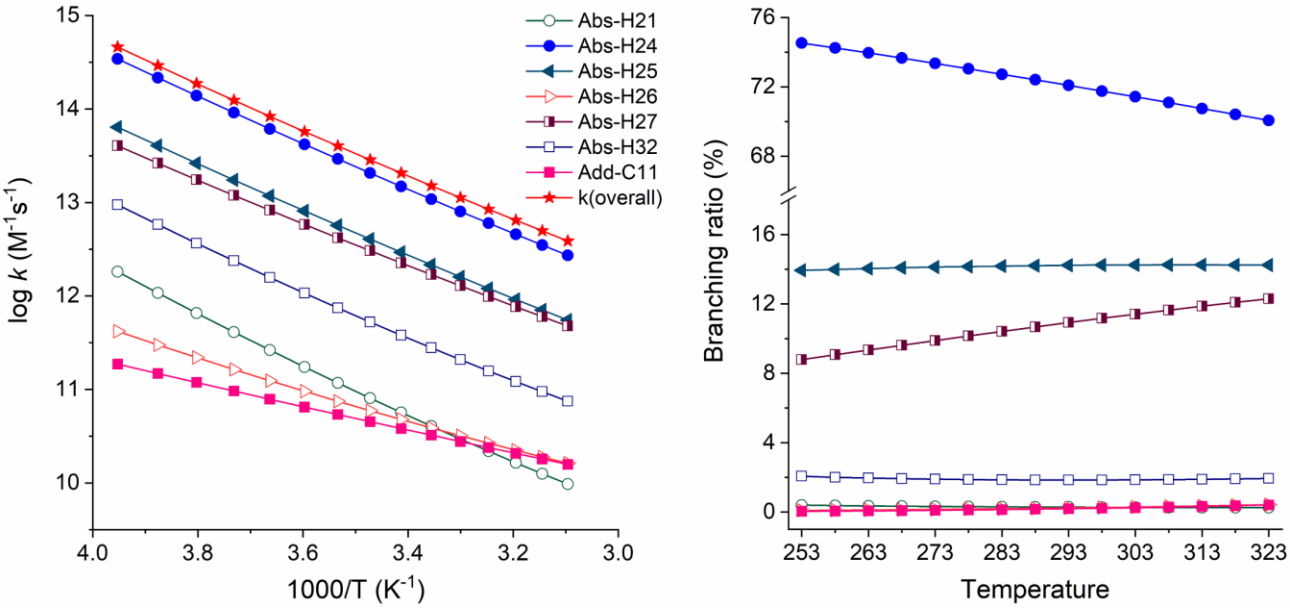

Figure 9: Influence of temperature on the overall rate constants as log k (M^{-1} s^{-1}) and branching ratio Γ (%) for main abstraction and addition reactions of MTZ oxidation by $SO_4^{\bullet-}$ radical in gas at 253-323 K temperature range.

When the temperature increases, the degradation of MTZ by $SO_4^{\bullet-}$ in the gas phase becomes slower. The $k_{overall}$ value reduces more than 100 times, from 4.59×10^{14} to 3.87×10^{12} M^{-1} s^{-1} with the temperature increase from 253 to 323 K.

4. HAT or PCET

Hydrogen transfer reactions may occur *via* two pathways: hydrogen atom transfer (HAT) and proton-coupled electron transfer (PCET).[72–75] In HAT reactions, the proton and the electron are transferred together as a single entity, *i.e.*, a hydrogen atom. Meanwhile, in PCET ones, these species are concertedly transferred in a single step, without any stable intermediate, but as two separated particles. To determine the chemical nature of this process, the singly occupied molecular orbital (SOMO) (**Figure 10)** and chemical parameters, including atomic charge, spin, and natural electron configuration (NEC) (**Table 2**), are considered. Furthermore, only the fastest reaction at each C-alkyl

is performed. In water, the Abs-H20, Abs-H26, Abs-H27, and Abs-H33 hydrogen abstraction reactions are investigated. Meanwhile, the ones in gas are Abs-H21, Abs-H24, Abs-H27, and Abs-H32, respectively.

Figure 10 presents structures and SOMO orbitals of the TS of Abs-H20, Abs-H26, Abs-H27, and Abs-H33 reactions in water. In principle, it has broadly been accepted that the significant part of the SOMO orbital of the HAT-TS is distributed in a straight line along the C···H···O transition vector, with a node plane found at the H atom. Meanwhile, the SOMO of the PCET-TS is located far from the reactive site of the reaction, and it is spread between the molecule and the radical, indicating the electron transfer route. This is the first signal allowing us to distinguish the TS of HAT or PCET reaction.

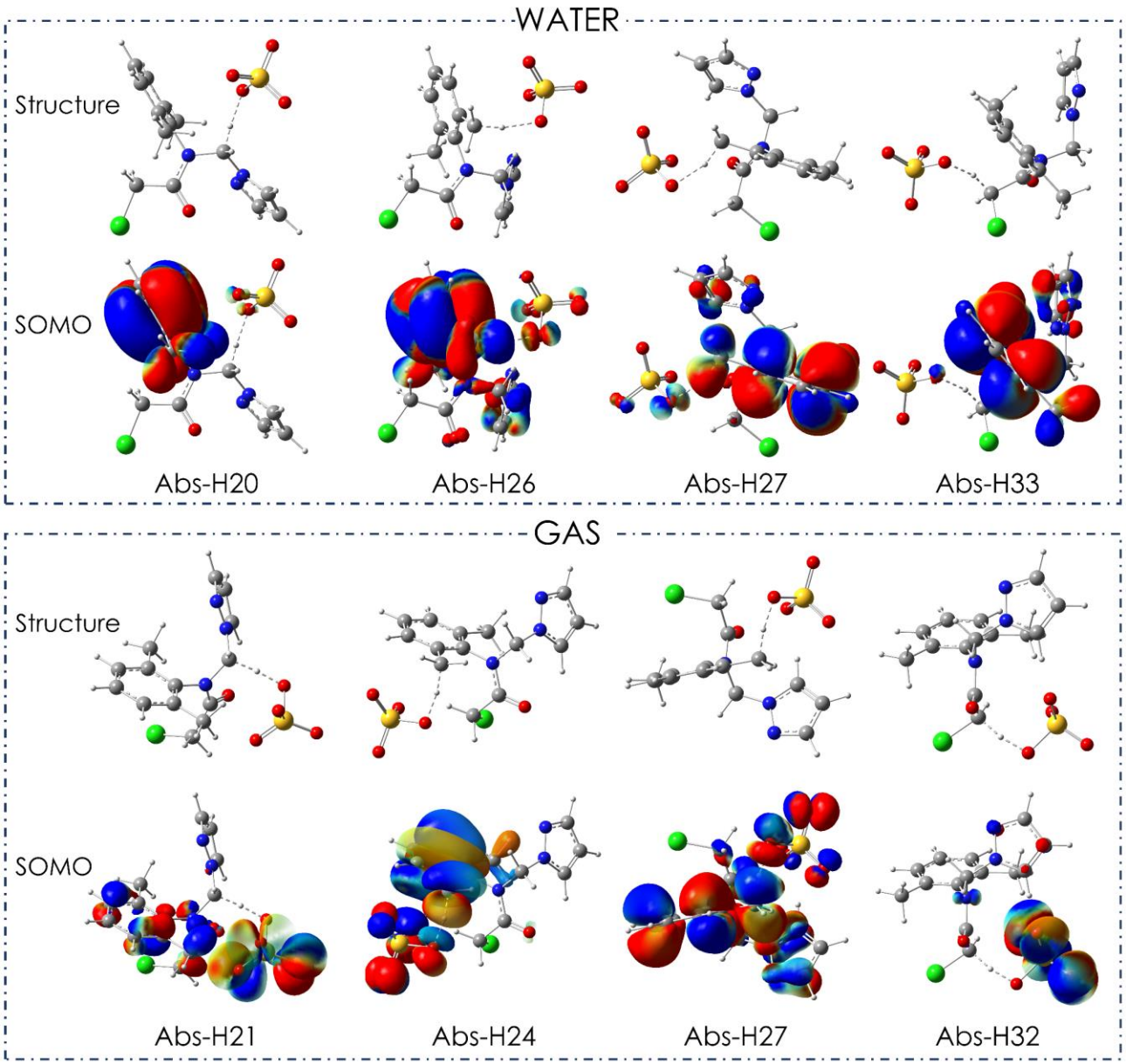

Figure 10. The structure and SOMO orbital of the transition state (TS) of the most favorable abstraction reactions of the degradation of MTZ by $SO_4^{\bullet-}$ radical in the water and gas phases.

The SOMO orbitals of Abs-H20 and H33 (of methyl groups) are almost absent at the reactive site C···H···O. Instead, the SOMOs of these structures mainly appear in the benzene rings. As a result, the proton and the electron are transferred *via* two separate pathways as the characteristics of the PCET mechanism. In this PCET process, the proton is transferred from the C-H bond to the O atom, whereas the electron is moved from the benzene ring to the other O atom of $SO_4^{\bullet-}$ radical. Meanwhile, for the Abs-H26 and Abs-H27 (of methylene groups), although the SOMOs appear at the C···H···O sites, the overlaps at these structures are offset from the reactive vectors. Furthermore, SOMOs also appear at the benzene ring of a large size, like the Abs ones in H-methyl groups, which are projected to be the electron exchange sites. Therefore, the reactions are projected to occur *via* the PCET mechanism.

In addition, the atomic charges and spin densities of the transferred-H atom in water are also used to confirm the PCET mechanism of these reactions (**Table 2**). Indeed, the charges of the transferred-H atoms are all small and negligible, from 0.027 (Abs-H20) to 0.037 (Abs-H33). Meanwhile, spins of these atoms are also negligible, from 0.021 (Abs-H20) to 0.026 (Abs-H33), which corresponds to a natural electron configuration of type $1s^0$, indicating the chemical nature of the proton instead of atomic hydrogen. This is suitable with some reports in the literature[72–74].

To conclude, the PCET is determined to be the mechanism of the hydrogen abstraction reaction in the $SO_4^{\bullet-}$ degradation of MTZ in water.

Table 2. Hirshfeld charge, spin density, and natural electron configuration (NEC) of the transition state of the most favorable abstraction reactions of the degradation of MTZ by $SO_4^{\bullet-}$ radical in the water and gas phase

WATER					GAS				
Position		Donator	Hydrogen	Acceptor	Position		Donator	Hydrogen	Acceptor
H20	Charge	0.069	0.027	-0.204	H21	Charge	0.071	0.041	-0.205
	Spin	0.122	0.021	0.563		Spin	0.260	0.021	0.468
	NEC	$2s^0\ 2p^1$	$1s^0$	$2s^1\ 2p^2$		NEC	$2s^1\ 2p^2$	$1s^0$	$2s^1\ 2p^2$
H26	Charge	-0.063	0.030	-0.208	H24	Charge	-0.069	0.038	-0.206
	Spin	0.126	0.023	0.569		Spin	0.215	0.020	0.525
	NEC	$2s^1\ 2p^2$	$1s^0$	$2s^1\ 2^2$		NEC	$2s^1\ 2p^2$	$1s^0$	$2s^1\ 2p^2$
H27	Charge	-0.076	0.032	-0.202	H27	Charge	-0.067	0.037	-0.200
	Spin	0.132	0.024	0.591		Spin	0.219	0.021	0.535
	NEC	$2s^1\ 2p^2$	$1s^0$	$2s^1\ 2p^2$		NEC	$2s^1\ 2p^2$	$1s^0$	$2s^1\ 2p^2$
H33	Charge	0.012	0.037	-0.191	H32	Charge	0.008	0.043	-0.197
	Spin	0.210	0.026	0.523		Spin	0.263	0.018	0.505
	NEC	$2s^1\ 2p^2$	$1s^0$	$2s^1\ 2p^2$		NEC	$2s^1\ 2p^2$	$1s^0$	$2s^1\ 2p^2$

Regarding reactions in the gas phase, the PCET is also observed as the mechanism of the Abs reaction. Indeed, like the Abs reactions in water, the SOMOs of the TS of Abs-H21 and Abs-H32 (at methyl groups) are found far from the C···H···O transition vector. Meanwhile, for the Abs-24 and Abs-H27 reactions (at methylene groups), the SOMOs have located a part at the C···H···O transition vector but with a bent angle of about 100^o, and the other significant part of the SOMOs is found at benzene ring. This indicates that the electron transfer process is expected to occur at a different route

from the proton transfer. In addition, charges, and spins of the transferred-H species are also negligible, which vary from 0.037 (Abs-H27) to 0.041 (Abs-H21), 0.018 (Abs-H32) to 0.021 (Abs-H21 and H27). In addition, all the natural electron configurations (NEC) are likely to be type $1s^0$. Thus, the hydrogen species of the TSs in the gas have many characteristics of a proton. As a result, the mechanism of these Abs reactions is PCET.

In conclusion, the Abs reaction at H atoms in the $SO_4^{\bullet-}$ degradation of MTZ occurs *via* the PCET reaction. In these reactions, the proton is transferred throughout the C···H···O vector, whereas the electron is shifted elsewhere, from the benzene ring to the sulfate radical anion.

5. Discussion

To evaluate the effectiveness of the $SO_4^{\bullet-}$-based degradation of MTZ, the rate constants of reactions initiated by $SO_4^{\bullet-}$, $HO^{\bullet}$ [7], and O_3 [76] calculated at the same level of theory are compared. **Figure 12** demonstrates rate constants (log *k*) of MTZ degradation by $SO_4^{\bullet-}$, $HO^{\bullet}$ [7], and O_3 [76] in water and the gas phase at the temperature of 283-323K and 253-323K, respectively. Among them, the degradation of MTZ by O_3 in the gas phase is evaluated from 283 to 323 K.[76]

As can be seen, the rate constants of the reaction initiated by $SO_4^{\bullet-}$ are much faster than that of $HO^{\bullet}$ and O_3 in both water and gas. Indeed, the $SO_4^{\bullet-}$ - initiated degradation in the water is about 18 and 53 times higher than that of the $HO^{\bullet}$ one at 283 K and 323 K, respectively. Meanwhile, this degradation is also around 8×10^7 and 8×10^6 times faster than the O_3-degradation reactions at the same temperature range, respectively. Regarding the gas phase, the $SO_4^{\bullet-}$ - initiated degradation is about 6000-226 times faster than that of $HO^{\bullet}$ at 253-323 K and around $5 \times 10^{12} - 10^{11}$ times as much as that of O_3 one at 283-323 K, respectively.

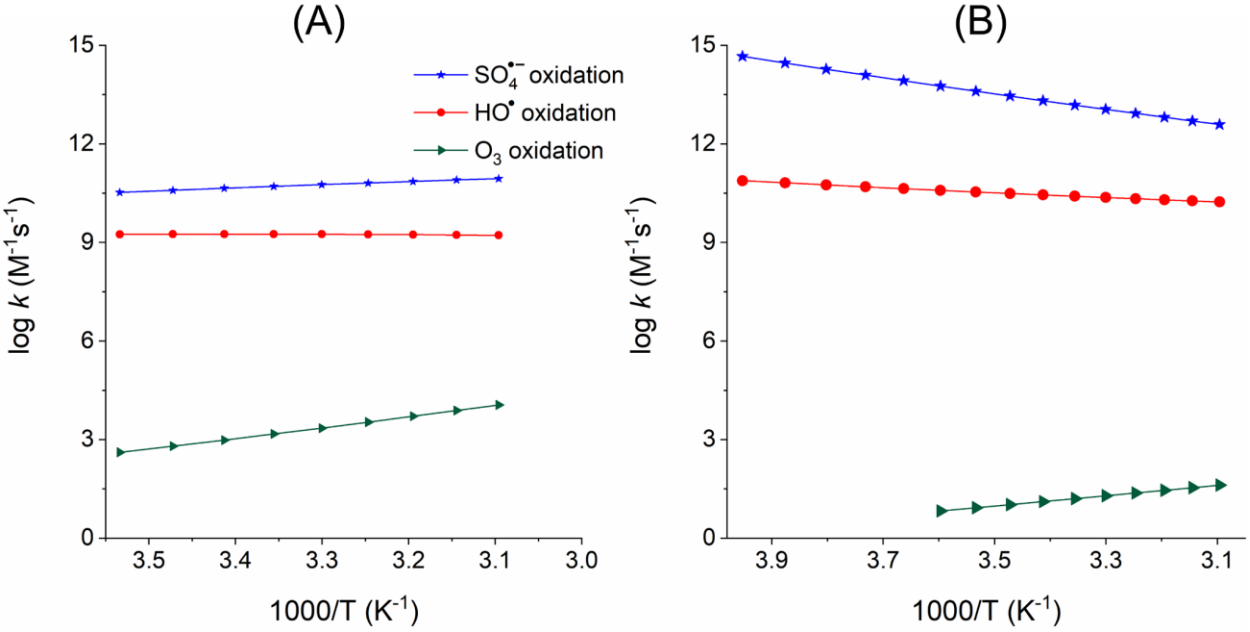

Figure 12. Comparison of MTZ degradations by $SO_4^{\bullet-}$, $HO^{\bullet}$ radicals, and O_3 in the water (A) and gas (B) phases.

Overall, the degradation of MTZ using $SO_4^{\bullet-}$ is expected to be significantly faster and more efficient than that by $HO^{\bullet}$ and O_3 in both gas and water. As a result, the SR-AOP is expected to be a highly advanced oxidation process for MTZ and similar compounds.

Conclusions

The mechanism and kinetics of the initial oxidation of metazachlor by sulfate radical anion in the influence of temperature have been investigated using density functional theory – DFT. The conclusions are multiple as follows:

- The degradation of MTZ by $SO_4^{\bullet-}$ radicals occurs *via* three mechanisms, including abstraction, addition, and single electron transfer. In water, all reactions are favorable and spontaneous with low energy barriers. Meanwhile, in the gas phase, Abs and Add reactions are more predominant, while the SET ones are negligible.
- The kinetics of degradation reactions in the water and gas phases at 298.15K have been determined. $SO_4^{\bullet-}$ is extremely reactive in the MTZ degradation in both water and gas. In water, the SET is the fastest reaction with the k_{app} = 5.76 × 10^9 M^{-1} s^{-1} and Γ = 11.39%. Therefore, when MTZ contacts the $SO_4^{\bullet-}$ in the solution, the MTZ^+ cation is expected to be the firstly formed product, which may further react with oxidizing agents in the aqueous environment. Besides, the Abs and Add reactions occurs in a non-selective manner, in which Γ varies from 3.34% (Add-C18) to 5.01% (Abs-H26). On the contrary, the degradation in gas is highly selective mostly *via* the Abs reactions, with the most dominant reaction being Abs-H24 with k_{app} = 1.08 × 10^{13} M^{-1} s^{-1} and Γ = 71.76% at 298K. The most significant elementary reaction in the gas phase reduces in the order: Abs-H24 (Γ, 71.76%) >> Add-C11 (0.21%) >> SET (0.00%).
- The influence of temperature on the degradation reactions has been investigated. The degradation in water becomes faster and more favorable, with the rate constant varying from 3.31 × 10^{10} (283K) to 8.76 × 10^{10} M^{-1} s^{-1} (323K), due the strong increase of the diffusion rate. In contrast, the decreasing trend is observed in the gas phase, with the rate constant from 4.59 × 10^{14} (253K) to 3.87 × 10^{12} M^{-1} s^{-1} (323 K), which is explained as the remarkable decline of the equilibrium constant ($K_{A,B}$).
- The total rate constant of degradation in water is many times lower than that in the gaseous phase, e.g., at 298.15K, k_{total} being 5.06 × 10^{10} and 1.51 × 10^{13} M^{-1} s^{-1}, respectively. The main reasons of this phenomenon are the influence of the diffusion effect of water and the extremely high thermal rate constants of main reactions in both phases.
- Regarding the chemical nature of Abs reaction, the most dominant Abs reactions occurring at H species of methyl and methylene groups of MTZ compound are observed to occur *via* the PCET mechanism in both water and gas phases. Indeed, in analyzing the SOMO, atomic charge, spin densities, and NECs of TS structure, we proved that the H-transferred species have the proton nature.
- The rate of degradation of MTZ by $SO_4^{\bullet-}$ radicals is compared with those by $HO^{\bullet}$ radicals and O_3. The total rate constant of the degradation by $SO_4^{\bullet-}$ radical anions is much larger than ones

by the HO radical and O_3. As a result, the SR-AOP is expected to be a potential and effective method for the degradation of MTZ.

Hopefully, the obtained results shed more light on the oxidation process of pesticides using sulfate radical anion, which is highly prospective and active.

REFERENCES

1 X. Duan, X. Niu, J. Gao, S. Wacławek, L. Tang and D. D. Dionysiou, *Curr. Opin. Chem. Eng.*, 2022, **38**, 100867.
2 M. Malakootian, A. Shahesmaeili, M. Faraji, H. Amiri and S. Silva Martinez, *Process Saf. Environ. Prot.*, 2020, **134**, 292–307.
3 F. Ghanbari and M. Moradi, *Chem. Eng. J.*, 2017, **310**, 41–62.
4 A. Derbalah and H. Sakugawa, *Sulfate Radical-Based Advanced Oxidation Technology to Remove Pesticides From Water A Review of the Most Recent Technologies*, Springer International Publishing, 2024, vol. 18.
5 X. Xia, F. Zhu, J. Li, H. Yang, L. Wei, Q. Li, J. Jiang, G. Zhang and Q. Zhao, *Front. Chem.*, 2020, **8**.
6 D. H. Truong, T. L. A. Nguyen, N. Alharzali, H. K. Al Rawas, S. Taamalli, M. Ribaucour, H. L. Nguyen, A. El Bakali, T. C. Ngo, I. Černušák, F. Louis and D. Q. Dao, *Chemosphere*, 2024, **350**, 141085.
7 D. Q. Dao, S. Taamalli, F. Louis, D. Kdouh, Z. Srour, T. C. Ngo, D. H. Truong, V. Fèvre-Nollet, M. Ribaucour, A. El Bakali and I. Černuśák, *Chemosphere*, 2023, **312**, 137234.
8 A. Derbalah, A. Ismail, A. Hamza and S. Shaheen, *Water Environ. Res.*, 2014, **86**, 584–593.
9 V. A. Sakkas, D. A. Lambropoulou and T. A. Albanis, *Chemosphere*, 2002, **48**, 939–945.
10 D. Manos, K. Miserli and I. Konstantinou, *Catalysts*, 2020, **10**, 1–44.
11 B.-T. Zhang, Y. Zhang, Y. Teng and M. Fan, *Crit. Rev. Environ. Sci. Technol.*, 2015, **45**, 1756–1800.
12 A. TSITONAKI, B. PETRI, M. CRIMI, H. MOSBÆK, R. L. SIEGRIST and P. L. BJERG, *Crit. Rev. Environ. Sci. Technol.*, 2010, **40**, 55–91.
13 P. Hu and M. Long, *Appl. Catal. B Environ.*, 2016, **181**, 103–117.
14 Q. Zhao, Q. Mao, Y. Zhou, J. Wei, X. Liu, J. Yang, L. Luo, J. Zhang, H. Chen, H. Chen and L. Tang, *Chemosphere*, 2017, **189**, 224–238.
15 S. Giannakis, K.-Y. A. Lin and F. Ghanbari, *Chem. Eng. J.*, 2021, **406**, 127083.
16 L. He, H. Chen, L. Wu, Z. Zhang, Y. Ma, J. Zhu, J. Liu, X. Yan, H. Li and L. Yang, *Ecotoxicol. Environ. Saf.*, 2021, **208**, 111522.
17 H. Lebik-Elhadi, Z. Frontistis, H. Ait-Amar, F. Madjene and D. Mantzavinos, *Process Saf. Environ. Prot.*, 2020, **134**, 197–207.
18 N. Genç and E. Durna, *Environ. Prog. Sustain. Energy*, 2018, **37**, 1632–1637.
19 Y. Lu, Y. Liu, C. Tang, J. Chen and G. Liu, *Processes*, 2022, **10**, 941.
20 K. Wei, A. Armutlulu, Y. Wang, G. Yao, R. Xie and B. Lai, *Appl. Catal. B Environ.*, 2022, **303**, 120889.
21 W. Hayat, Z. Liu, Y. Wan and Y. Zhang, *Environ. Technol. Innov.*, 2022, **26**, 102352.
22 J. Deng, M. Xu, Y. Chen, J. Li, C. Qiu, X. Li and S. Zhou, *Chem. Eng. J.*, 2019, **366**, 491–503.
23 W. Wang, M. Chen, D. Wang, M. Yan and Z. Liu, *Sci. Total Environ.*, 2021, **772**, 145522.
24 Z. Shen, H. Zhou, P. Zhou, H. Zhang, Z. Xiong, Y. Yu, G. Yao and B. Lai, *J. Hazard. Mater.*, 2022, **425**, 127781.
25 C. Cai, S. Kang, X. Xie and C. Liao, *J. Hazard. Mater.*, 2020, **385**, 121519.
26 A. Santos, J. Fernandez, S. Rodriguez, C. M. Dominguez, M. A. Lominchar, D. Lorenzo and A. Romero, *Sci. Total Environ.*, 2018, **615**, 1070–1077.
27 J. Tan, Z. Li, J. Li, Y. Meng, X. Yao, Y. Wang, Y. Lu and T. Zhang, *J. Hazard. Mater.*, 2022, **423**, 127048.
28 W. Zheng, Y. Sun and Y. Gu, *J. Hazard. Mater.*, 2022, **436**, 129058.
29 M. Amasha, A. Baalbaki and A. Ghauch, *Chem. Eng. J.*, 2018, **350**, 395–410.
30 Y. Liu, L. Liu and Y. Wang, *Environ. Sci. Technol.*, 2021, **55**, 9691–9710.

31 Y. Liu, J. Zhou, Y. Zhang, J. Pan, Q. Wang and J. Zhang, *Fuel*, 2015, **145**, 180–188.
32 X. Ma, R. Hao, Z. Wang, P. Xu, Y. Luo and Y. Zhao, *Chem. Eng. J.*, 2020, **401**, 126101.
33 R. Xie, J. Ji, K. Guo, D. Lei, Q. Fan, D. Y. C. Leung and H. Huang, *Chem. Eng. J.*, 2019, **356**, 632–640.
34 R. Xie, J. Cao, X. Xie, D. Lei, K. Guo, H. Liu, Y. Zeng and H. Huang, *Chem. Eng. J.*, 2020, **401**, 126077.
35 L. He, L. Bu, R. Spinney, D. D. Dionysiou and R. Xiao, *Environ. Res.*, 2021, **201**, 111523.
36 M. Xu, J. Yao, S. Sun, S. Yan and J. Sun, *Toxics*, 2021, **9**, 234.
37 H. V. Lutze, S. Bircher, I. Rapp, N. Kerlin, R. Bakkour, M. Geisler, C. Von Sonntag and T. C. Schmidt, *Environ. Sci. Technol.*, 2015, **49**, 1673–1680.
38 Q. Mei, J. Sun, D. Han, B. Wei, Z. An, X. Wang, J. Xie, J. Zhan and M. He, *Chem. Eng. J.*, 2019, **373**, 668–676.
39 X. Bo, J. Sun, Q. Mei, B. Wei, Z. An, Z. Qiu, D. Han, J. Xie and M. He, *J. Clean. Prod.*, 2021, **293**, 126161.
40 S. Luo, Z. Wei, D. D. Dionysiou, R. Spinney, W. P. Hu, L. Chai, Z. Yang, T. Ye and R. Xiao, *Chem. Eng. J.*, 2017, **327**, 1056–1065.
41 W. Liu, G. Lv, X. Sun, L. He, C. Zhang and Z. Li, *Ecotoxicol. Environ. Saf.*, 2019, **183**, 109551.
42 D. Wang, Y. Li, M. Yang and M. Han, *Sci. Total Environ.*, 2008, **393**, 64–71.
43 S. Mohr, R. Berghahn, M. Feibicke, S. Meinecke, T. Ottenströer, I. Schmiedling, R. Schmiediche and R. Schmidt, *Aquat. Toxicol.*, 2007, **82**, 73–84.
44 F. L. Dixon, D. V. Clay and I. Willoughby, *Crop Prot.*, 2006, **25**, 259–268.
45 M. Kask, M. Krichevskaya and J. Bolobajev, *J. Environ. Chem. Eng.*, 2019, **7**, 103095.
46 G. Weber, N. Christmann, A.-C. Thiery, D. Martens and J. Kubiniok, *Sci. Total Environ.*, 2018, **619**–**620**, 638–648.
47 V. Kodes and M. Rieder, in *Managing Watersheds for Human and Natural Impacts*, American Society of Civil Engineers, Reston, VA, 2005, pp. 1–5.
48 P. Karier, G. Kraus and I. Kolber, *Environ. Sci. Eur.*, 2017, **29**, 25.
49 U. Ulrich, G. Hörmann, M. Unger, M. Pfannerstill, F. Steinmann and N. Fohrer, *Sci. Total Environ.*, 2018, **618**, 26–38.
50 L. Mayer, C. Degrendele, P. Šenk, J. Kohoutek, P. Přibylová, P. Kukučka, L. Melymuk, A. Durand, S. Ravier, A. Alastuey, A. R. Baker, U. Baltensperger, K. Baumann-Stanzer, T. Biermann, P. Bohlin-Nizzetto, D. Ceburnis, S. Conil, C. Couret, A. Degórska, E. Diapouli, S. Eckhardt, K. Eleftheriadis, G. L. Forster, K. Freier, F. Gheusi, M. I. Gini, H. Hellén, S. Henne, H. Herrmann, A. Holubová Šmejkalová, U. Hõrrak, C. Hüglin, H. Junninen, A. Kristensson, L. Langrene, J. Levula, M. Lothon, E. Ludewig, U. Makkonen, J. Matejovičová, N. Mihalopoulos, V. Mináriková, W. Moche, S. M. Noe, N. Pérez, T. Petäjä, V. Pont, L. Poulain, E. Quivet, G. Ratz, T. Rehm, S. Reimann, I. Simmons, J. E. Sonke, M. Sorribas, R. Spoor, D. P. J. Swart, V. Vasilatou, H. Wortham, M. Yela, P. Zarmpas, C. Zellweger Fäsi, K. Tørseth, P. Laj, J. Klánová and G. Lammel, *Environ. Sci. Technol.*, 2024, **58**, 3342–3352.
51 J. Jurčíková, P. Mikula, R. Dobšíková, D. Némethová and Z. Svobodová, *Acta Vet. Brno*, 2007, **76**, S61–S66.
52 O. Işik, E. Sarihan, E. Kuşvuran, Ö. Gül and O. Erbatur, *Aquaculture*, 1999, **174**, 299–311.
53 J. Velisek, A. Stara, J. Kubec, E. Zuskova, M. Buric and A. Kouba, *Sci. Rep.*, 2020, **10**, 1–9.
54 M. J. Frisch, G. W. Trucks, H. B. Schlegel, G. E. Scuseria, M. A. Robb, J. R. Cheeseman, G. Scalmani, V. Barone, G. A. Petersson, H. Nakatsuji, X. Li, M. Caricato, A. V. Marenich, J. Bloino, B. G. Janesko, R. Gomperts, B. Mennucci, H. P. Hratchian, J. V. Ortiz, A. F. Izmaylov, J. L. Sonnenberg, D. Williams-Young, F. Ding, F. Lipparini, F. Egidi, J. Goings, B. Peng, A. Petrone, T. Henderson, D. Ranasinghe, V. G. Zakrzewski, J. Gao, N. Rega, G. Zheng, W. Liang, M. Hada, M. Ehara, K. Toyota, R. Fukuda, J. Hasegawa, M. Ishida, T. Nakajima, Y. Honda, O. Kitao, H. Nakai, T. Vreven, K. Throssell, J. A. J. Montgomery, J. E. Peralta, F. Ogliaro, M. J. Bearpark, J. J. Heyd, E. N. Brothers, K. N. Kudin, V. N. Staroverov, T. A. Keith, R. Kobayashi, J. Normand, K. Raghavachari, A. P. Rendell, J. C. Burant, S. S. Iyengar, J. Tomasi, M. Cossi, J. M. Millam, M. Klene, C. Adamo, R.

Cammi, J. W. Ochterski, R. L. Martin, K. Morokuma, O. Farkas, J. B. Foresman and D. J. Fox, *Gaussian 16, Revision A.03*, Gaussian, Inc., Wallingford CT, 2016.
55 A. V Marenich, C. J. Cramer and D. G. Truhlar, *J. Phys. Chem. B*, 2009, **113**, 6378–6396.
56 D. L. Singleton and R. J. Cvetanović, *J. Am. Chem. Soc.*, 1976, **98**, 6812–6819.
57 A. Miyoshi, GPOP software, rev. 2022.01.20m1, available from the author., http://akrmys.com/gpop/.
58 A. Galano and J. R. Alvarez-Idaboy, *J. Comput. Chem.*, 2013, **34**, 2430–2445.
59 S. Canneaux, F. Bohr and E. Henon, *J. Comput. Chem.*, 2014, **35**, 82–93.
60 R. A. Marcus, *J. Chem. Phys.*, 1956, **24**, 966–978.
61 R. A. Marcus, *J. Chem. Phys.*, 1957, **26**, 872–877.
62 R. A. Marcus, *J. Chem. Phys.*, 1957, **26**, 867–871.
63 F. C. Collins and G. E. Kimball, *J. Colloid Sci.*, 1949, **4**, 425–437.
64 M. v. Smoluchowski, *Zeitschrift für Phys. Chemie*, 1918, **92U**, 129–168.
65 S. Pamidighantam, S. Nakandala, E. Abeysinghe, C. Wimalasena, S. R. Yodage, S. Marru and M. Pierce, *Procedia Comput. Sci.*, 2016, **80**, 1927–1939.
66 N. Shen, Y. Fan and S. Pamidighantam, *J. Comput. Sci.*, 2014, **5**, 576–589.
67 R. Dooley, K. Milfeld, C. Guiang, S. Pamidighantam and G. Allen, *J. Grid Comput.*, 2006, **4**, 195–208.
68 K. Milfeld, C. Guiang, S. Pamidighantam and J. Giuliani, *Proc. 2005 Linux Clust. HPC Revolut.*, 2005.
69 J. Yang, W.-L. You, D. You, L. Zheng, J. Jin and S.-L. Luo, *Chemosphere*, 2024, **363**, 142953.
70 M. Mahdi Ahmed, S. Barbati, P. Doumenq and S. Chiron, *Chem. Eng. J.*, 2012, **197**, 440–447.
71 Y. Chen, M. Li, Y. Tong, Z. Liu, L. Fang, Y. Wu, Z. Fang, F. Wu and L. Z. Huang, *Chem. Eng. J.*, 2019, **368**, 495–503.
72 D. H. Truong, T. H. Lan Nguyen and D. Q. Dao, *R. Soc. Open Sci.*, , DOI:10.1098/rsos.230114.
73 A. Martínez, A. Galano and R. Vargas, *J. Phys. Chem. B*, 2011, **115**, 12591–12598.
74 J. M. Mayer, D. A. Hrovat, J. L. Thomas and W. T. Borden, *J. Am. Chem. Soc.*, 2002, **124**, 11142–11147.
75 A. Galano, *J. Mex. Chem. Soc.*, 2017, **59**, 231–262.
76 C.-T. Phan Dang, D. H. Truong, T. L. A. Nguyen, S. Taamalli, A. El Bakali, F. Louis and D. Q. Dao, *Environ. Sci. Pollut. Res.*, 2024, **31**, 49427–49439.